ISSN 1063-7826, Semiconductors, 2010, Vol. 44, No. 9, pp. 1199–1210. © Pleiades Publishing, Ltd., 2010.
Original Russian Text © V.V. Strelchuk, V.P. Kladko, E.A. Avramenko, O.F. Kolomys, N.V. Safryuk, R.V. Konakova, B.S. Yavich, M.Ya. Valakh, V.F. Machulin, A.E. Belyaev, 2010, published in Fizika i Tekhnika Poluprovodnikov, 2010, Vol. 44, No. 9, pp. 1236–1247.

LOW-DIMENSIONAL SYSTEMS

X-ray Diffraction Analysis and Scanning Micro-Raman Spectroscopy of Structural Irregularities and Strains Deep Inside the Multilayered InGaN/GaN Heterostructure

V. V. Strelchuk[a]^, V. P. Kladko[a], E. A. Avramenko[a], O.F. Kolomys[a], N. V. Safryuk[a], R. V. Konakova[a], B. S. Yavich[b]^^, M. Ya. Valakh[a], V. F. Machulin[a], and A. E. Belyaev[a]

[a] *Lashkaryov Institute of Semiconductor Physics, National Academy of Sciences of Ukraine, Kyiv, 03028 Ukraine*
^e-mail: Strelch@isp.kiev.ua
[b] *ZAO Svetlana-Optoelectronics, St. Petersburg, 194156 Russia*
^^e-mail: byavich@soptel.ru

Submitted December 7, 2009; accepted for publication December 14, 2009

Abstract—High-resolution X-ray diffraction analysis and scanning confocal Raman spectroscopy are used to study the spatial distribution of strains in the $In_xGa_{1-x}N$/GaN layers and structural quality of these layers in a multilayered light-emitting diode structure produced by metal–organic chemical vapor deposition onto (0001)-oriented sapphire substrates. It is shown that elastic strains almost completely relax at the heterointerface between the thick GaN buffer layer and $In_xGa_{1-x}N$/GaN buffer superlattice. It is established that the GaN layers in the superlattice are in a stretched state, whereas the alloy layers are in a compressed state. In magnitude, the stretching strains in the GaN layers are lower than the compressive strains in the InGaN layers. It is shown that, as compared to the buffer layers, the layers of the superlattice contain a smaller number of dislocations and the distribution of dislocations is more randomly disordered. In micro-Raman studies on scanning through the thickness of the multilayered structure, direct evidence is obtained for the asymmetric gradient distributions of strains and crystal imperfections of the epitaxial nitride layers along the direction of growth. It is shown that the emission intensity of the $In_xGa_{1-x}N$ quantum well is considerably (more than 30 times) higher than the emission intensity of the GaN barrier layers, suggesting the high efficiency of trapping of charge carriers by the quantum well.

DOI: 10.1134/S1063782610090174

1. INTRODUCTION

In recent years, the amount of new data on the III–N nanostructures have increased. This is promoted by the improvement of the methods of growth of nitrides and by the development of new nitride-based device structures. The quantum-confined InGaN/GaN heterostructures are widely used for production of visible and ultraviolet light sources [1, 2]. One of the serious problems in production of high-quality III–N heterostructures is that no sufficiently inexpensive GaN substrates needed for the homoepitaxial growth are available. Therefore, as a rule, the III–N compounds are epitaxially deposited onto substrates (Al_2O_3 [3], 6*H*-SiC [4], Si [5]) such that the resulting layer–substrate system exhibits a large lattice mismatch between the components and a noticeable difference between their coefficients of thermal expansion. As a consequence, considerable elastic strains are produced in the nitride layers. The epitaxial growth under high strains is accompanied by the formation of a spontaneous piezoelectric field, a column-like layer structure [6, 7], and structural defects (dislocations, domain boundaries, etc.) with a high concentration [8, 9]. In addition, possible fluctuations of the process parameters (the temperature and rate of deposition, the ratio between the fluxes of elements) during the growth of the structure, surface segregation of indium [8], and mixing of the components at the quantum well–barrier heterointerface [9] have a profound effect on the degree of crystalline homogeneity of the epitaxial film. The above-mentioned factors impede reproducible fabrication of perfect epitaxial III–N heterostructures with specified physical properties. For this reason, the studies of the effect of irregularities of the crystal structure in the lateral plane and through the thickness of the nitride layers on their phonon spectra and emission properties present a topical problem. In the case of strained (In, Ga)N structures, only a limited number of attempts were made to correlate the optical properties of the structures with their nanoscaled local structural and morphological features [10]. Specifically, it was shown that the localization of excitons and/or charge carriers, when trapped at deep energy states induced by compositional fluctuations in the $In_xGa_{1-x}N$ alloy, resulted in the efficient suppression of nonradiative recombination centers [11]. Transmission electron microscopy (TEM) was used for the study of structural defects and

the distribution of strains in depth in the epitaxial layers of the multilayered (InGa)N/GaN structure [12]. It was shown [13] that, during the growth of the short-period InGaN/GaN superlattice, nanodomains 3–15 nm in dimension can be formed, with the density $\geq 10^{11}$ cm^{-2} and the periodically modulated ratio between the components.

Only a few data have been reported on the studies of the $In_xGa_{1-x}N$ crystals and epitaxial layers by Raman spectroscopy. Raman studies of the InGaN/GaN structures excited by ultraviolet radiation allowed the observation of irregularities in composition and strains in the epitaxial $In_xGa_{1-x}N$ layers [10, 14].

Confocal micro-Raman spectroscopy has not been practically used for the studies of structural irregularities in nitride layers. This nondestructive optical method does not call for special preparation of samples and provides a means for directly analyzing elastic strains, structural imperfections, and components in quantum-confined nanoheterostructures at a quantitative level with a submicrometer spatial resolution. Recently, confocal micro-Raman spectroscopy was applied to studies of the distribution of strains in depth for the GaN layer in an $AlGaN/GaN/Al_2O_3$ nanostructure by step-by-step scanning from the surface of the heterostructure to the interface between the epitaxial layer and the substrate [15].

X-ray diffraction (XRD) analysis of multilayered systems is used to determine their structural parameters, such as the composition and thickness of individual layers and the order of their arrangement [7, 16–20]. Analysis of XRD curves makes it possible to describe the degree of abruptness of heterointerfaces, the strains and structural quality of epitaxial layers, the content of components, the types of defects, etc.

In this paper, we report the results of studies of the emission properties and the distributions of elastic strains and structural imperfections in depth in the heteroepitaxial nitride layers of the InGaN/GaN multilayered structure with the $In_xGa_{1-x}N$ quantum wells (QWs) by the XRD analysis, confocal micro-Raman spectroscopy, and photoluminescence (PL) measurements. The structure was grown on a single-crystal sapphire substrate. When scanning through the thickness of the InGaN/GaN structure, we observe a profound enhancement of inelastic scattering at the A_1^{LO} phonons of the $In_xGa_{1-x}N$ QWs, a shift of the A_1^{LO} mode to lower frequencies, and an asymmetric broadening of the phonon line as compared to the high-frequency mode of symmetry E_2 (E_2^{high}). The experimentally observed changes in the micro-Raman spectra are attributed to the selective resonance excitation of different local regions of the structure with different In content in (InGa)N QWs [17]. The gradient distribution of elastic strains and structural imperfections in depth in the epitaxial nitride layers is established. The results are of importance for the technology of growth of epitaxial nitride layers and for prediction of the physical properties of optoelectronic devices based on such materials.

2. EXPERIMENTAL

The light-emitting AlGaInN diode structures studied here were fabricated by metal–organic chemical vapor deposition (MOCVD) onto (0001)-oriented sapphire substrates. On the sapphire surface, we successively formed a low-temperature GaN nucleation layer, on which we grew a thick *n*-GaN buffer layer (with the thickness $d \sim 3.5$ μm). To reduce the mismatch strains and the density of misfit dislocations in the layers of the active region of the $In_xGa_{1-x}N$/GaN structure, we grew a five-period $In_xGa_{1-x}N$(2.5 nm)/GaN(4 nm) buffer superlattice (SL) with a low In content in the $In_xGa_{1-x}N$ QWs on the GaN buffer layer. The SL of the active region consisted also of five $In_xGa_{1-x}N$ layers (with the thickness $d_{InGaN} = 2.5$ nm) separated by GaN barriers (with the thickness $d_{GaN} = 9$ nm). Over the active region, we grew a thin current-limiting p-$Al_{0.15}Ga_{0.85}N$ layer with the thickness 15–20 nm. On this layer, we deposited a *p*-GaN contact layer with the thickness 0.1 μm and with the concentration of holes $N_p > 2 \times 10^{17}$ cm^{-3}.

The XRD studies of the samples were conducted with the use of a PANalytical X'Pert PRO MRD high-resolution diffractometer. We studied (000*l*) symmetric and $(\bar{1}\bar{1}24)$ asymmetric reflections. The experimental layouts allowed us to study two sections of reciprocal lattice sites, specifically, the section orthogonal to the diffraction vector (ω scanning) and the section parallel to the diffraction vector (ω/2θ scanning). The three-axis XRD study makes it possible to separate the effects associated with changes in the interplanar spacing and the effects associated with rotation of atomic planes; therefore, from analysis of the distribution of the intensity in the system of coordinate axes (q_z, q_x) directed, correspondingly, along and perpendicularly to the diffraction vector **H**, it is possible to determine the contribution of each of the above-mentioned effects to the structural changes separately [20, 21]. Macroscopic strains responsible for bending of the samples were estimated from the radius of curvature of the system. The radius of curvature was determined from the changes in the angle of reflection from sapphire on linear scanning of the sample along the X-ray beam. In the study, we used the following parameters of the layers: $a = (3.1896 \pm 0.0003)$ Å, $c = (5.1855 \pm 0.0002)$ Å, $c/a = (1.6258 \pm 0.0002)$, and $p = 2c_{13}/c_{33} = 0.53$ for GaN [18] and $a = (3.5378 \pm 0.0001)$ Å, $c = (5.7033 \pm 0.0001)$ Å, $c/a = (1.6121 \pm 0.0001)$, and $p = 2c_{13}/c_{33} = 0.49$ for InN [19]. The theoretical analysis of the diffraction reflectivity spectra was accomplished in the context of the semicinematic

Parameters of the layers of SLs

Layers of structures		t, nm	c, nm	a, nm	ε_{zz}	x	c/a
SL1	$In_xGa_{1-x}N$	3.6	0.52987	0.32309	0.01410	0.18	1.6400
	GaN	8.9	0.51744	0.31871	–0.00561	–	1.6235
SL2	$In_xGa_{1-x}N$	3.5	0.53007	0.32313	0.01560	0.07	1.6404
	GaN	3.8	0.51713	0.31887	–0.00645	–	1.6217

Note: SL1 is the SL of the active region, and SL2 is the buffer SL.

approximation [20] and the procedure described elsewhere [21].

The micro-Raman spectra were obtained at room temperature in the backscattering layout of measurements with the use of a Horiba Jobin Yvon T64000 spectrometer with a confocal microscope (the 100× lens, the 0.90 aperture). The spectra were recorded with a cooled CCD detector. The Raman and PL spectra were excited with Ar–Kr laser radiation (at the excitation wavelength λ_{exc} = 488.0 nm) and He–Cd laser radiation (at λ_{exc} = 325.0 nm), respectively. In the Raman measurements, the laser beam was focused into a spot of diameter <1 μm at the sample. The spatial (lateral and in-depth) mapping of phonon spectra of the epitaxial layers of the structure was accomplished by moving the piezoelectrically controlled objective table with a step of ~0.1 μm. The accuracy of determining the phonon line frequency was 0.15 cm^{-1}. To avoid heating or degradation of the sample, we varied the laser radiation power from 0.5 to 2 mW corresponding to the power density 50–200 kW cm^{-2} at the sample surface.

3. RESULTS AND DISCUSSION

3.1 XRD Data for Multilayered Structures

Figure 1 shows the experimental diffraction reflectivity curves (DRCs) for the 0002 symmetric reflection in the InGaN/GaN multilayered structure as obtained in the two- (curve *1*) and three-crystal (curve *2*) schemes of measurements and the theoretically calculated DRC (curve *3*). The DRCs present two sets of satellites, of which the more-pronounced set (S_n) corresponds to the basic SL and the set of a smaller number of satellites with a lower intensity (S'_n) to the buffer SL. In Fig. 1, the position of the zero satellite is masked by the peak of the GaN buffer layer with a high-intensity diffuse component.

In the DRCs of the SLs, we can see two systems of oscillations, i.e., two periodical distributions of the intensity as a function of the angle of incidence; specifically, we can see "fast" oscillations typical of reflection from a thin layer or from the entire structure and periodically arranged satellites (S_n) of up to the second order, which are indicative of the good periodicity of the structures. In the experimental DRC, we can see the splitting of the zero satellite, which is impossible to attribute to oscillations of the thickness. As shown by the results of simulation, the splitting is the effect of the coating layer responsible for reflection in the region of the zero satellite of the basic SL. It is impossible to determine the In content in the QWs of the buffer SL from the experimental spectra, since this spectrum falls within the region of the effect of both the zero satellite of the basic SL and the reflection peaks of the coating layer and GaN buffer layer. The issue concerning the In content in the QW of the buffer SL can be clarified only by simulating the spectra of the structure. The simulation yields the In content at a level of ~(8–10)%.

Using the DRC curves for the SLs, we can directly determine the SL period T from the angular separation between satellites $\delta\theta$:

$$T = \frac{|\gamma_h|\lambda}{\sin(2\theta_B)\delta\theta}. \quad (1)$$

Here, λ = 1.54056 Å is the X-ray wavelength. We can also directly determine the average interplanar spacing

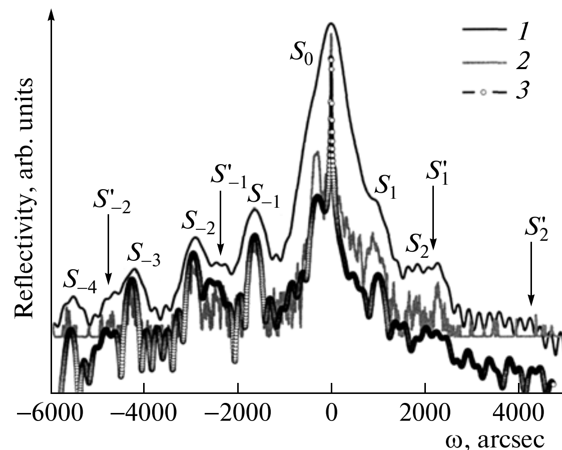

Fig. 1. Experimental ω–2θ scans obtained in (*1*) the two- and (*2*) three-crystal schemes for the symmetric 0002 reflection of the $In_xGa_{1-x}N$/GaN SL grown on the GaN buffer layer and (*3*) the calculated spectrum. S_n are the satellites of the active SL, and S'_n are the satellites of the buffer SL.

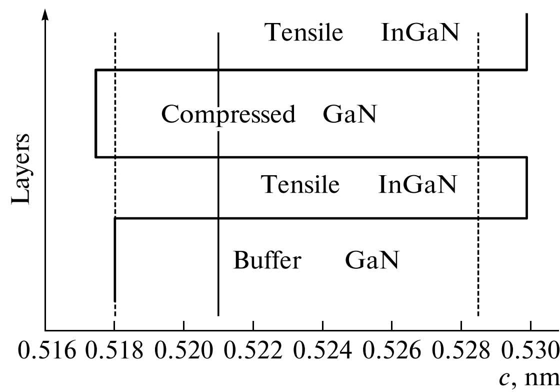

Fig. 2. Schematic diagram of the distribution of the lattice parameter c in depth for the strained $In_xGa_{1-x}N$/GaN SL on the GaN buffer layer. Dashed lines mark the parameter c for unstrained layers, and the solid line marks the parameter c averaged over the SL period.

$\langle d \rangle$ from the angular separation between the peak related to the substrate and the central peak (zero satellite) related to the SL:

$$(\Delta d/d)_{zz} = \frac{\langle d \rangle - d_0}{d_0} = -\Delta\theta\Big/\left[(\tan\theta_B)\frac{2|\gamma_h|}{\gamma_0 + |\gamma_h|}\right]. \quad (2)$$

In relations (1) and (2), γ_0 and γ_h are the directional cosines for the incident and diffracted beams, $(\Delta d/d)_{zz}$ is the lattice mismatch between the SL and the substrate in the plane orthogonal to the direction of growth of the structure, and d_0 is the spacing between the crystallographic planes of the substrate.

For epitaxial structures belonging to the hexagonal system and grown on the (0001) surface, we have

$$(\Delta d/d)_{zz} = \Delta c/c + p(\Delta a/a), \quad (3)$$

where $p = 2c_{13}/c_{33}$ (c and a are the parameters of the hexagonal unit cell). The above parameters suffice to determine the parameters of SLs consisting of pure materials.

It should be noted that, in the DRCs for nitride films grown on sapphire, there is no peak of the substrate to serve as a reference peak in the determination of strains in the epitaxial buffer layers (the nearest reflection peak of sapphire is several degrees from the region of angles studied here). For this reason, determining the parameters a and c requires referencing to the absolute scale of angles of reflection. The referencing was accomplished by measuring the scattering angle 2θ for the GaN layer and for the central peak of the SL with the use of an analyzer.

For defect structures, to which the system studied here belongs, the satellites are broadened because of the influence of defects [22]. However, experience shows that all satellites of the SL are distorted in a similar manner (if only defects rather than deviations from the periodicity are taken into account). This allows one to correlate the calculated curves (for an ideal SL) with the experimental (distorted) reflection curves by comparing the relative heights of the satellites or their integrated intensities.

The parameters of the multilayered structure are obtained from the simulation of the reflectivity spectra by the method described in [21] and refined by fitting the calculated curves to the experimental ones (see table).

When expression (2) is used, it is important to be sure that the epitaxial layers have coherent boundaries and that the system is not relaxed. Elastic strains (mainly mismatch-related and thermal strains) can relax via various mechanisms [23], of which the basic mechanism is the generation of misfit dislocations. In this case, along with the normal mismatch $(\Delta d/d)_{zz}$, there is the tangential mismatch $(\Delta d/d)_{xx}$ (for nonrelaxed systems, the spacing between the planes orthogonal to the heterointerface is the same for all of the layers and the substrate). In the rocking curves, the relaxation is evident as an angular shift of diffraction peaks and their broadening in comparison to peaks for the elastically strained system. However, from the angular position of the symmetric Bragg reflection peaks, it is impossible to infer whether a particular layer is in the elastically strained state or in the relaxed state if the composition of the layer is not known in advance. By recording the asymmetric reflections, we obtained the average value $\langle a \rangle$ of the SL parameter a: $\langle a \rangle = (a_1t_1 + a_2t_2)/T$. Here, a_1 and a_2 are the parameters of the unit cell and t_1 and t_2 are the thicknesses of the individual layers of the SL. Using a similar formula, we determined the average value $\langle c \rangle$ of the SL parameter c from the symmetric reflections.

Then, with the quantities B (B is the parameter proportional to the ratio between the thicknesses of the individual layers of the SL), $\langle c \rangle$, and $\langle a \rangle$, we determined the real parameters c_i and a_i for both layers of the SL, after which we determined the In content in the InGaN layer and the distribution of the parameter c through the thickness of the SL. All of the results are given in the table and Fig. 2.

The three-crystal geometric layout of diffraction makes it possible to gain an insight into the relaxation of epitaxial structures from analysis of the so-called reciprocal space maps (RSMs), i.e., the maps of distributions of the intensity around the sites of the reciprocal space [17]. The approach is based on the fact that, in the plane of scattering, the intensity of coherent scattering from totally strained epitaxial heterostructures is distributed in the direction normal to the surface.

In this direction, there are the supplementary sites, i.e., the centers of reflection from individual layers, oscillations of the thickness, and the SL-related satellites. Relaxation is recorded in the maps of distributions of the intensity around the reciprocal lattice sites corresponding to the asymmetric Bragg reflections,

for which the diffraction vector makes an angle φ with the normal **n**. For the totally relaxed structure, the sites, the centers of reflection from individual layers, are bound to lie along the diffraction vector. If relaxation is partial, the sites are in some intermediate positions. Thus, if centers corresponding to two neighboring layers or to one layer and the substrate lie along the normal **n** on the maps of distributions of the intensity, there has been no relaxation between these layers, and the heterointerface is coherent. Otherwise, the map is indicative of relaxation. Recording of the distribution of the intensity around the 0002 reciprocal lattice site by means of three-crystal diffractometry shows the periodic character of the distribution in the direction normal to the sample surface (Fig. 3a). However, the preceding is inadequate to analyze the degree of relaxation for the symmetric RSMs. Figure 3b shows the RSM for the $11\bar{2}4$ site. In Fig. 3b, q_x and q_y are coordinates in the reciprocal space.

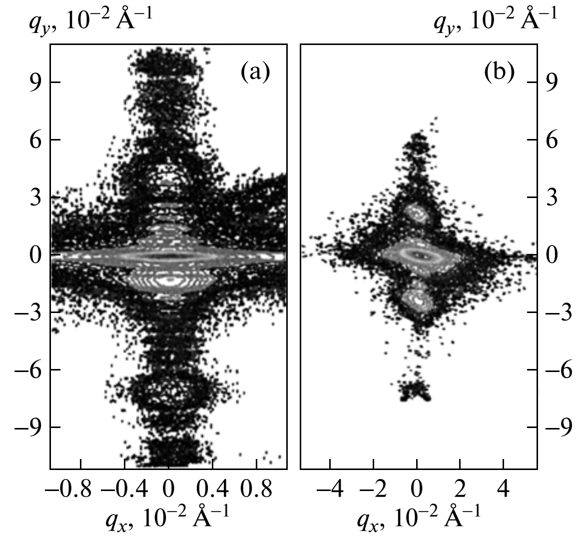

Fig. 3. Distributions of the intensity around the reciprocal lattice sites (a) 0002 and (b) $11\bar{2}4$ in the strained $In_xGa_{1-x}N$/GaN SL.

Relaxation is complete if the sites lie along the direction of the reciprocal lattice vector **H**. In the case under study, the SL-related sites (satellites) lie along the normal to the surface, although the entire set of satellites is shifted by some distance with respect to those of the GaN buffer layer. The active SL was grown on the buffer SL with a lower In content. This means that the SR structure was grown on the buffer layer relaxed to some extent. Since the III–N films grown on sapphire relax practically completely at the temperature of growth and, hence, the strains observed in the films at room temperature are basically thermal in nature, we can infer that this is true also for the buffer layer. In this case, we can describe the relaxation of the SL using two relaxation parameters that correspond to relaxation of the SL as a whole with respect to the buffer layer and to relaxation of individual layers with respect to each other.

As for the complete relaxation of the buffer layer, it is related to the lattice parameters of this layer in the free state and is defined with respect to the substrate (the centers of reflection from the layer and the substrate lie along the direction of **H**). It is worth noting that these considerations refer to structures belonging to the hexagonal system for which the ratio c/a = 1.633 typical of the close-packed arrangement is retained in all layers.

The $In_xGa_{1-x}N$/GaN SLs studied here feature a rather large (>1%) lattice mismatch between the neighboring layers, the relatively small layer thicknesses, and the small total SL thickness.

For wurtzite structures (among which are the InGaN and GaN crystal structures) that grow along the ⟨0001⟩ hexagonal axis, the lattice parameter a defines the interplanar spacing in the plane of the heterointerface and the parameter c defined the spacing in the direction orthogonal to the interface. Let a_i and c_i denote the experimentally determined lattice parameters of the ith layer in the system and let a_i^b and c_i^b denote the corresponding parameters of the layer of the same composition in the free (unstrained) state. Here, the subscript $i = 0$ corresponds to the buffer layer and $i = 1$ and 2 to the first and second layers of the SL. The elastic strain of the layers of the SL is

$$\varepsilon_i = \frac{a_i - a_i^b}{a_i^b}, \tag{4}$$

and the real parameter c_i is $c_i = c_{ib}(1 - p\varepsilon_i)$, where $p = 2c_{13}/c_{33}$ is the Poisson ratio. Relaxation of elastic strains in the SL can be described by the step $\Delta a_i = a_i - a_{i-1}$ of the lattice parameter a at the heterointerface or by the relative relaxation level,

$$r_i = \frac{a_i - a_{i-1}}{a_i^b - a_{i-1}} = \frac{\Delta a_i}{a_i^b - a_{i-1}}. \tag{5}$$

The quantities Δa_1 and r_1 correspond to relaxation at the lower heterointerface (between the buffer layer and the first layer of the SL), and the quantities Δa_2 and r_2 correspond to relaxation at the interfaces between individual layers (Fig. 4). For the strained coherent structure, we have $\Delta a_1 = \Delta a_2 = 0$ and, consequently, $r_i = 0$; for the relaxed layers, we have $r_i = 1$.

If the coherence of the individual layers of the SL is retained and the SL relaxes as a whole with respect to the buffer layer, we have $\Delta a_2 = 0$, whereas Δa_1 can be below zero as well as above zero, depending on the composition of the buffer layer. In the general case of a relaxed incoherent SL, both steps of the lattice

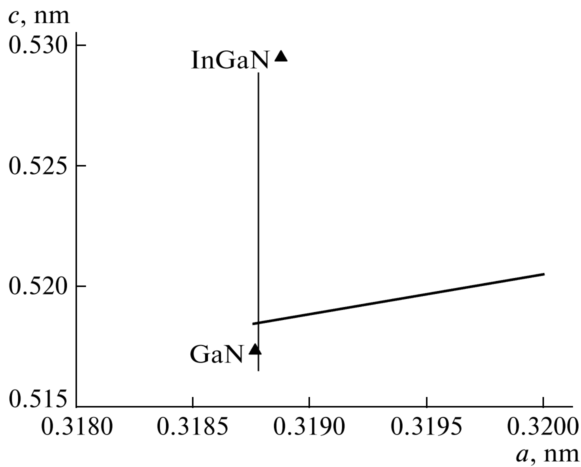

Fig. 4. Lattice parameters a and c for the layers of the strained $In_xGa_{1-x}N/GaN$ SL. The sold line corresponds to the relaxed parameters calculated by Vegard's law.

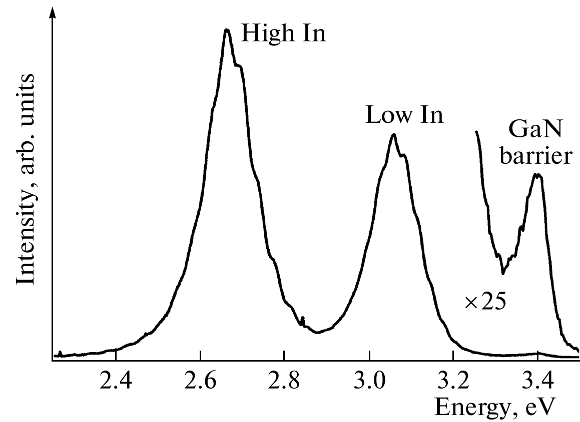

Fig. 5. PL spectra of the multilayered InGaN/GaN structure. λ_{exc} = 325 nm. The measurement temperature is 300 K.

parameters differ from zero; in this case, the periodicity of the structure is retained, if the magnitudes of Δa_0 are identical at all interfaces between the layers of the SL.

From the table and Fig. 2, it is evident that, in the SLs of the multilayered structure studied here, the GaN layers are stretched in the plane orthogonal to the direction of growth ($\varepsilon_{xx} > 0$), whereas the InGaN alloy layers are compressed ($\varepsilon_{xx} < 0$). The fact that the stretching strains in the GaN layers are smaller than the compressive strains in the InGaN alloy layers is caused mainly by the thickness of the layers of the SLs. In addition, for all of the multilayered InGaN/GaN structures, we observe almost complete relaxation of elastic strains at the lower heterointerface between the thick GaN buffer layer (d_{GaN} = 3 μm) and the $In_xGa_{1-x}N$ layers of the buffer SL ($\langle x \rangle = 0.08$), since their lattice mismatch is larger than the critical mismatch ($\Delta a/a \approx 0.476\%$).

The epitaxial layers differ from single crystals in their defect structure, since the main source of generation of defects in the layers is presented by the relaxation of elastic misfit strains arising from the lattice mismatch between the film and the substrates or between individual layers [15]. The structure of layers exhibits a more ordered arrangement of defects, highly anisotropic fields of shear strains, and clearly pronounced directions parallel to the surface of the crystal wafer (heterointerfaces) and normal to the surface.

It is known that the epitaxial nitride layers grown on sapphire substrates exhibit a high density of threading dislocations ($\sim 10^{10}$ cm^{-2}) responsible for substantial broadening of diffraction reflection peaks (Fig. 3). Broadening of the intensity distribution on the RSMs in the direction orthogonal to the diffraction vector **H** is also due to average rotations of domains and their finite effective lateral dimension, and broadening along the vector **H** is due to strains inside the domains and their finite dimensions along the normal **n**. As follows from Fig. 3, the diffraction pattern is broadened mainly in the direction parallel to the surface, whereas the broadening in the normal direction is much less pronounced [17]. Dislocation networks localized at the heterointerface also induce some broadening of the diffraction pattern in the direction orthogonal to the reciprocal lattice vector, irrespective of the direction of this vector (Fig. 3b). The dislocation structure of the SLs composed of nitride layers is in many respects identical to the dislocation structure of single-layered nitride films [24].

As to the dislocation structure of the layers of the SL, the analysis shows that the layers exhibit a lower density of dislocations and a more random distribution of dislocations. The minor role of dislocation in the layers of the SL is supported also by the unstrained state of the SL with respect to the buffer layer.

Thus, as follows from the X-ray data, the epitaxial layers constituting the SLs exhibit a lower density of dislocations than the buffer layers do. In all of the SLs, we observe relaxation at the lower heterointerface; i.e., the strains produced between the buffer SL as a whole and the GaN buffer layer are removed. The main SL is strained with respect to the buffer SL.

3.2 Results of Optical Studies

Figure 5 shows the PL spectra of the multilayered InGaN/GaN structure at room temperature. In the spectra, we observe a low-intensity emission band at the photon energy $h\nu \approx 3.4$ eV, with the full width at half-maximum (FWHM) $\Gamma \approx 0.08$ eV. The band corresponds to the region of fundamental absorption of the GaN buffer and barrier layers. In addition, in the PL spectrum, we observe intense and, at the same time, rather broad emission bands corresponding to recombination of electron–hole pairs in the QWs of

the SL active region of the $In_xGa_{1-x}N$/GaN structure ($h\nu \approx 3.06$ eV, $\Gamma \approx 0.12$ eV) and in the QWs of the $In_xGa_{1-x}N$/GaN buffer SL ($h\nu \approx 2.66$ eV, $\Gamma \approx 0.13$ eV). The energy position of these PL bands corresponds to the difference between the energies of the ground size-quantization states of electrons in the conduction band (E_{e1}) and heavy holes in the valence band (E_{hh1}), with the correction for the exciton binding energy.

By analyzing the energy position of the PL bands of the $In_xGa_{1-x}N$ QWs, we estimated the average In content in the active and buffer SLs from the dependence of the band gap E_g on the composition parameter x of the $In_xGa_{1-x}N$ alloy [25], $E_g(x) = 3.493 - 2.843x - bx(1 - x)$, where $b = 2.5$ eV. In this case, for the $In_xGa_{1-x}N$ QW of the $In_xGa_{1-x}N$/GaN buffer SL, the PL band with a peak at $h\nu \approx 3.06$ eV corresponds to $x = 0.08$; at the same time, the PL band at $h\nu \approx 2.66$ eV corresponds to emission from the $In_xGa_{1-x}N$ QW of the active $In_xGa_{1-x}N$/GaN SL with $x = 0.18$. This result is in good agreement with the XRD data (see table).

The broadening observed in the PL spectrum for the emission band of the $In_xGa_{1-x}N$ QWs is caused by the nonuniform spatial distribution of indium and residual strains and by fluctuations of the thickness of the QW and barrier layers [26]. Such spatial irregularities of structural parameters are responsible for local potential fluctuations and density-of-states tails formed near the conduction and valence band edges. In this case, the annihilation of excitons localized in the minima of potential fluctuations makes the major contribution to the emission band of the InGaN QWs [27]. Therefore, analysis of the shape of the broad emission bands of the $In_xGa_{1-x}N$ QWs provides only a few data and makes impossible unambiguous characterization of the shape of a particular well. However, the emission intensity of the $In_xGa_{1-x}N$ QWs (with the width 2.5 nm) is much (more than 30 times) higher than the emission intensity of the GaN barriers layers ($h\nu \approx 3.4$ eV), suggesting that the capture of charge carriers by such QWs is highly efficient.

To study the structural properties of the multilayered light-emitting AlGaInN diode structure, we used micro-Raman spectroscopy as a nondestructive method of studies of quantum-confined heterosystems.

The GaN and InN single crystals and $In_xGa_{1-x}N$ alloys are highly stable in the hexagonal wurtzite phase and belong to the space group C^4_{6v}. The group-theoretical analysis predicts that, in the center of the Brillouin zone (the point Γ), there exist optical modes: $\Gamma_{opt} = A_1(Z) + 2B + E_1(X, Y) + 2E_2$, where X, Y, and Z are polarization directions [28]. The $A_1(Z)$ and $E_1(X, Y)$ modes are polar, split into the longitudinal optical (LO) and transverse optical (TO) components, and are active in the Raman and infrared spectra. The

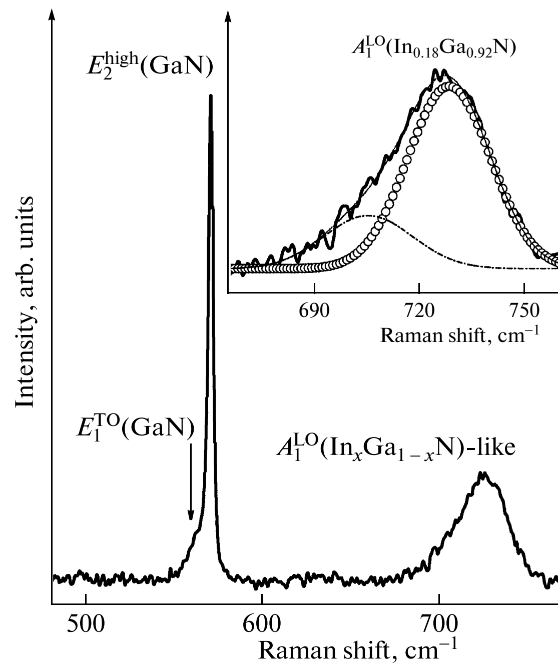

Fig. 6. The micro-Raman spectrum of the multilayered InGaN/GaN structure. $\lambda_{exc} = 488.0$ nm ($E_{exc} = 2.54$ eV). The measurement temperature is 300 K.

two modes of the symmetry E_2, i.e., the E_2^{high} and E_2^{low} modes are active only in the Raman spectra, whereas the modes of the symmetry B (silent modes) are inactive in optical spectra. For the wurtzite structure, in the backscattering layout of experiments $Z(X, X + Y)\bar{Z}$, scattering at the E_2 and A_1^{LO} phonons is allowed [29].

Figure 6 exemplifies the Raman spectrum of the multilayered InGaN/GaN structure in the backscattering layout of experiment $Z(X, X + Y)\bar{Z}$, where the Z axis is directed along the c axis of the wurtzite structure. The spectrum is recorded at the excitation photon energy $E_{exc} = 2.54$ eV (the excitation wavelength is $\lambda_{exc} = 488.0$ nm). The experimental conditions provided the maximal signal intensity in the frequency region corresponding to scattering at the A_1^{LO} phonons of the $In_xGa_{1-x}N$ QWs.

On excitation with the photon energy $E_{exc} = 2.41$ eV ($\lambda_{exc} = 514.5$ nm), scattering at the A_1^{LO} phonons $In_xGa_{1-x}N$ is practically undetectable. This is indicative of the resonance character of excitation of compositionally inhomogeneous local regions in the nitride layers. Therefore, the frequency of the A_1^{LO} line may refer to the local region of the structure, where the In content deviates from the average content in the $In_xGa_{1-x}N$ QW. The conclusion that there are local

fluctuations of the distribution of indium follows also from the XRD data.

In the micro-Raman spectrum (Fig. 6), we observe an intense phonon band at the frequency ~570 cm^{-1} ($\Gamma = 2.54$ cm^{-1}). This band is allowed by the selection rules for the $Z(X, X)\bar{Z}$ layout of experiment and is defined by scattering at the nonpolar E_2^{high}(GaN) vibrations in the GaN coating and buffer layers of the structure. A slight frequency shift of the E_2^{high}(GaN) line with respect to the corresponding 569 cm^{-1} line in bulk GaN [30] is due to elastic strains in the epitaxial GaN layer ($\varepsilon_{zz} = -(5.4–6.8) \times 10^{-2}$), whereas the small FWHM of this line ($\Gamma \approx$ 2.5 cm^{-1}) demonstrates the rather high structural quality of the GaN layers [31]. The slightly pronounced low-frequency shoulder of the E_2^{high}(GaN) line at the frequency ~561 cm^{-1} refers to the E_1^{TO}(GaN) mode that is forbidden in the $Z(X, X)\bar{Z}$ layout of experiment by the selection rules, but appears in the spectrum due to the effects of disorder of the crystal structure (microscopic defects and structural irregularities). This conclusion is supported by the observation of the E_1^{TO}(GaN) mode in the $Y(X, Z)\bar{Y}$-polarized Raman spectra. It is interesting that the above-mentioned low-frequency shoulder of the E_2^{high}(GaN) mode is sometimes attributed to the E_2^{high}(InGaN) mode [32, 33]. From our point of view, such interpretation is ambiguous.

As can be seen from Fig. 6, in the frequency region of the A_1^{LO}(InGaN) vibrations (700–750 cm^{-1}), we observe a phonon band that has a complex shape. The procedure of fitting of the calculated curve to the experimental data allowed us to separate out a band at ~725 cm^{-1} (see inset in Fig. 6) corresponding to scattering at the A_1^{LO}($In_xGa_{1-x}N$) phonons of the active region of the InGaN/GaN structure [14]. The low-intensity band at ~705 cm^{-1} may refer to local regions with a high In content in the structure. It should be noted that, as a rule, the structural quality of the thin epitaxial $In_xGa_{1-x}N$ layers is low and, as a result, the A_1^{LO}(InGaN) Raman band is low in intensity and broadened. In the case under consideration, the study of the thin $In_xGa_{1-x}N$ QWs is possible due to the experimentally observed substantial enhancement of the scattering intensity in the region of the A_1^{LO}($In_xGa_{1-x}N$) mode at $E_{exc} = 2.54$ eV. This effect can be attributed to the resonance enhancement of Raman scattering at excitation energies close to the energies of real electron transitions. It can be expected that the random distribution of atoms of the alloy among the crystal lattice sites or the structural imperfections randomly dispersed in the crystal are responsible for shallow and deep energy states forming the Urbach exponential density-of-states tails of holes and electrons of the valence and conduction bands. Such an assumption is supported by rather intense anti-Stokes luminescence of the $In_xGa_{1-x}N$ QWs (not shown in Fig. 6) [34]. It should be noted that a similar resonance effect was observed for the A_1^{LO}(InN) band in the Raman spectra of InN [35], and although this effect was not interpreted, it is of interest for studies of very thin epitaxial $In_xGa_{1-x}N$ layers.

Before considering the structural homogeneity of the nitride layers over the thickness of the multilayered InGaN/GaN(0001) structure, let us analyze the effect of different physical factors on the width and phonon frequency of polar vibration bands in the Raman spectra of semiconductor nanostructures. The width of the phonon band is representative of the phonon decay anharmonicity, the degree of irregularity of the crystal structure, and the concentration of defects [36]. Natural fluctuations of the composition of alloys bring about the inhomogeneous broadening of phonon lines [37]. For wurtzite-structured semiconductors, polar modes can be broadened and shifted in frequency because of mixing of the A_1^{LO} and E_1^{LO} modes and the formation of quasi-phonons [38]. Different orientations of crystallites in polycrystalline nitride layers can be responsible for the extra broadening of phonon bands [39]. It is known that, in nanostructures, the quantum-confinement effect yields a shift of the phonon band to lower frequencies and an asymmetric broadening of the band due to phonon dispersion [40]. Finally, the fields of strains and the nonuniformity of these fields also influence the width and frequency position of phonon bands [41]. Therefore, in general, it is difficult to establish what effect of the above-listed ones is responsible for changes in the vibration spectrum when nanostructures are considered instead of bulk materials. However, on the basis of a thorough analysis of the above factors, it is possible to preclude some of them.

The confocal micro-Raman spectra of the InGaN/GaN structure are recorded with a high spatial resolution (~1 μm). Therefore, we can assume that the broadening of the phonon band due to disorientation of crystallites in a particular local region remains unchanged upon scanning the structure in depth. In this case, it is expected that the contribution of quasiphonons (that can be observed with the microscope lens with a wide aperture) to the broadening and frequency shift of the phonon band will be constant as well.

Let us now analyze the size-confinement effect on the polar modes of nanostructures with the axial anisotropy of the crystal structure. Since the A_1^{LO} phonon dispersion branch in nitrides is rather smooth

along the Γ–A direction [42], the size-confinement effect for phonons in nitride nanostructures is commonly insignificant. It was theoretically shown [43] that, for spheroidal wurtzite-structured quantum dots (QDs), the frequencies of polar optical phonons were independent of the absolute dimensions of the QDs. No confinement-induced changes in the frequency of the A_1^{LO} band were practically observed in the multilayered GaN/AlN QDs with the height ~3 nm (the change was $\Delta\omega_{conf} \le 0.2$ cm^{-1}) [44] and in the single-layer structure with the GaN QDs, for which the height-to-diameter ratio h/d_0 was ~1.8 nm/10.0 nm and ~2.5 nm/14 nm [45]. For this reason, in further analysis of the Raman spectra, we disregard the phonon size-confinement effect.

The $In_xGa_{1-x}N$ alloys, the crystal structure of which is hexagonal, exhibit the one-mode type of transformation of phonon spectra in the entire range of compositions from InN to GaN [31]. This means that the frequencies of all modes change continuously under changes in the composition of the alloy from InN to GaN. For the relaxed pseudomorphous crystalline $In_xGa_{1-x}N$ alloy films, the A_1^{LO} phonon frequency is determined from the relation [14]

$$\omega_0(x) = (736 \pm 1) - (149 \pm 2)x \tag{6}$$

and varies within the range of the A_1^{LO} phonon frequencies for the GaN and InN binary compounds (736–586 cm^{-1}).

For the strained wurtzite structure, the dependence of the phonon frequency ($\mathbf{q} = 0$) on biaxial strains in the plane of the layer perpendicular to the c axis is [14]

$$\Delta\omega(x) = 2a\varepsilon_{xx}(x) + b\varepsilon_{zz}(x) = [2a - b\nu]\varepsilon_{xx}(x). \tag{7}$$

Here, a and b are deformation constants for phonons, $\varepsilon_{xx}(x)$ and $\varepsilon_{zz}(x)$ are the nonzero components of the strain tensor, and $\nu = \varepsilon_{zz}(x)/\varepsilon_{xx}(x)$ is the Poisson ratio. The relations $2a - b\nu = \Delta\omega/\varepsilon_{xx} = (-10.5 \pm 3.1) \times 10^2$ cm^{-1} and $\Delta\omega/\varepsilon_{zz} = (-16.9 \pm 2.1) \times 10^2$ cm^{-1} [14] define the changes in the phonon frequency per unit strain. For GaN, $a(A_1^{LO}) = -782$ and $b(A_1^{LO}) = -1181$ cm^{-1} [46]. Since no data on the phonon deformation potential for the A_1^{LO} mode of InN are available in publications, we here use the value of the deformation potential for GaN.

Thus, for the pseudomorphous $In_xGa_{1-x}N$ layer, the phonon frequency is determined from the relation [14]

$$\omega^{pseudo}(x) = \omega_0(x) + \frac{\Delta\omega}{\varepsilon_{xx}(x)}(x)\varepsilon_{xx}(x). \tag{8}$$

Here, $\omega_0(x)$ is the phonon frequency for the unstrained $In_xGa_{1-x}N$ layer and $\varepsilon_{xx}(x) = [a^{pseudo} - a_0(x)]/a_0(x)$, where $a^{pseudo} = a(\text{GaN}) = 3.1892$ Å and $a_0(x)$ is the lattice constant determined for the unstrained $In_xGa_{1-x}N$ layer from Vegard's rule. It should be noted that the composition dependence of the quantity $\Delta\omega(x)/\varepsilon_{xx}(x)$ is unknown.

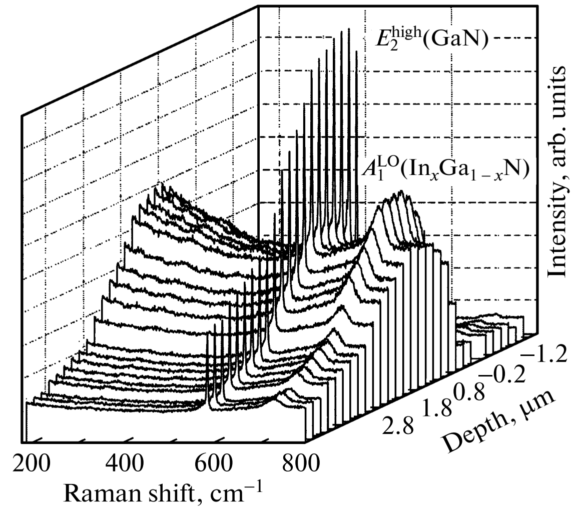

Fig. 7. Confocal micro-Raman spectra of the InGaN/GaN structure with quantum wells, as recorded upon scanning the structure in depth (along the crystallographic c axis, i.e., the axis of growth). $E_{exc} = 2.54$ eV ($\lambda_{exc} = 488.0$ nm). The measurement temperature is 300 K.

From relations (6) and (8) with the In content x and the strain $\varepsilon_{xx}(x)$ in the plane of the $In_xGa_{1-x}N$ layer of the active region, as determined from PL and X-ray studies, we determined the expected $A_1^{LO}(In_{0.18}Ga_{0.72}N)$-mode frequency shift $\Delta\omega$ induced by elastic strains in the layers: $\Delta\omega = 16.06 \pm 2$ cm^{-1}. The frequency determined from such calculations is in good agreement with the experimental frequency of the $A_1^{LO}(In_{0.18}Ga_{0.72}N)$ mode.

In other studies, the change in the $A_1^{LO}(In_{0.18}Ga_{0.72}N)$-mode frequency in the epitaxial $In_xGa_{1-x}N$ layer was attributed to the gradient of strains along the direction of growth of the structure [10], the selective resonance excitation of local regions different in In content, and the partial compensation under combined action of both effects [47].

Figure 7 shows the micro-Raman spectra of a multilayered InGaN/GaN QW structure as recorded for different depths (d) when moving the 100× lens of the microscope from the sample surface. The distance $d = 0$ corresponds to the spot focused at the structure surface, and $d = 4$ μm corresponds to the interface between the sapphire substrate and the GaN buffer layer. In the spectra, we detect an intense band corresponding to the E_2^{high}(GaN) mode (at ~570 cm^{-1}) and

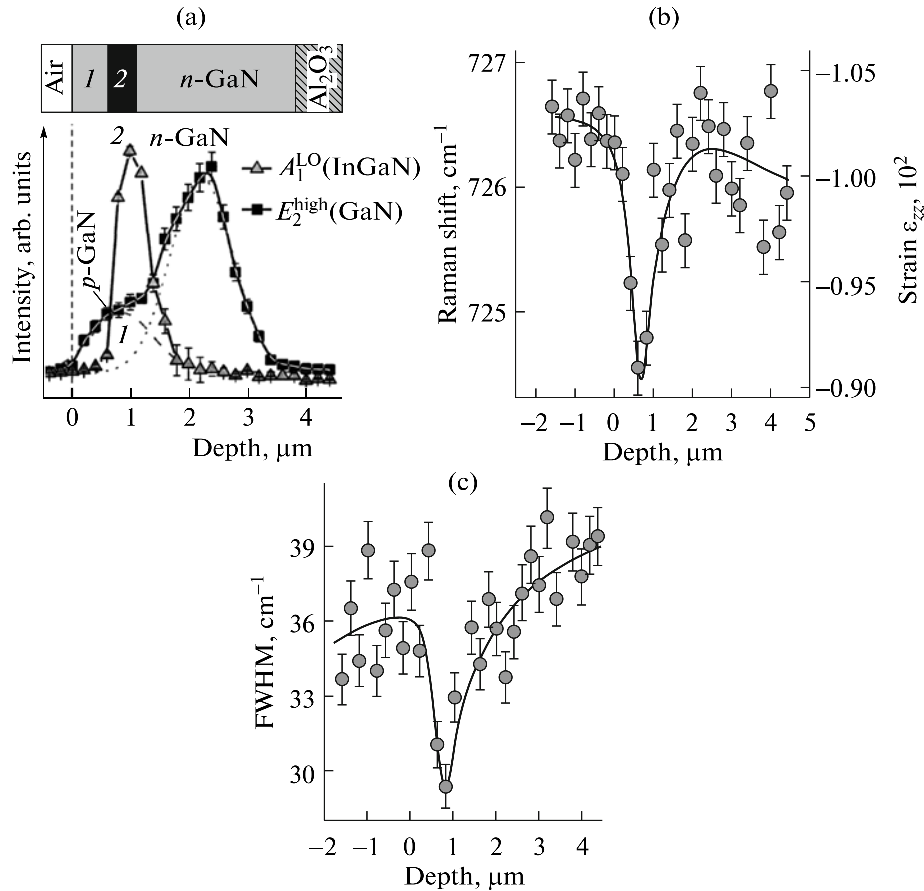

Fig. 8. Distributions of the parameters of the Raman band in depth inside the multilayered InGaN/GaN structure: (a) the intensities of the E_2^{high} mode in GaN and the A_1^{LO} mode in InGaN and (top) the schematic representation of the InGaN/GaN structure under study ((*1*) the thin *p*-GaN contact layer, (*2*) the InGaN/GaN SLs, and the thick *n*-GaN buffer layer are shown); (b) the frequency of the A_1^{LO} mode in InGaN and the elastic strain along the direction of growth of the multilayered structure; (c) the FWHM of the A_1^{LO} mode in the active $In_xGa_{1-x}N$ SL. E_{exc} = 2.54 eV (λ_{exc} = 488.0 nm). The measurement temperature is 300 K.

a band corresponding to the $A_1^{LO}(In_xGa_{1-x}N)$ mode (at ~725 cm^{-1}) of the active InGaN/GaN SL.

From Fig. 7, it can be seen that, as the depth of optical probing is varied and the active $In_xGa_{1-x}N$ SL is approached, we observe a resonance increase in the intensity of phonon bands in the Raman spectra. At the same time, the intensity of electron–hole recombination emission responsible for the high-energy region of the PL band of the $In_xGa_{1-x}N$ QWs at the excitation energy E_{exc} = 3.8 eV (Fig. 5). Such resonance enhancement of Raman scattering at the A_1^{LO} phonons was observed previously for doped $In_xGa_{1-x}N$ layers [48] and $In_{0.20}Ga_{0.80}N$/GaN SLs [49].

Figure 8a shows the variation in the intensities of vibration modes of the barrier GaN layers and $In_xGa_{1-x}N$ QWs on scanning from the sample surface to the heterointerface between the epitaxial layer and the substrate. The distribution of the intensity in depth exhibits two peaks, one at ~0.85 and the other at 2.4 μm, corresponding to the E_2^{high}(GaN) mode of the coating GaN layer and thick GaN barrier layer of the structure under study, respectively. At the same time, for the A_1^{LO}(InGaN) modes of two InGaN/GaN SLs, we also observe an asymmetric peak at ~1 μm (Fig. 8a) corresponding to the $In_xGa_{1-x}N$ QW of the active region of the light-emitting structure. The asymmetric wing to the right of the peak refers to the $In_xGa_{1-x}N$ QWs of the buffer SL; the low emission intensity in this region is indicative of the low structural quality of the SL that is found to be practically smeared (has no pronounced interfaces) in the structure. Thus, from the distribution shown in Fig. 8a, it is evident that systematic features of the variations in the intensity of phonon modes in depth within the multilayered

InGaN/GaN structure correspond closely to the architecture of the sample (see top of Fig. 8a).

Let us discuss in more detail the distributions of the frequency and FWHM of phonon lines in depth in the nitride layers of the InGaN/GaN structure (Figs. 8b, 8c). These distributions were obtained upon automated scanning of the multilayered structure in depth with the focused spot. The scan step was ~1 μm. In the measurements, the Raman signal intensity was averaged over a depth range no wider than ~500 nm. From the analysis of the parameters of the phonon band, it was possible to characterize the spatial distribution of elastic strains and the structural quality of the nitride layers. From Figs. 8b and 8c, it is evident that, if we focus the spot in the region of the $In_xGa_{1-x}N$ QW of the active SL, we observe a shift of the $A_1^{LO}(In_xGa_{1-x}N)$ mode to lower frequencies and a decrease in the FWHM of this mode (in Fig. 8b, we have $\Delta\omega \approx 2.5$ cm^{-1} and $\Delta\Gamma \approx 9.0$ cm^{-1}).

The total thickness of the InGaN QWs studied here is only ~(30–40) nm. Nevertheless, upon scanning the structure in depth, we reliably detect variations in the phonon spectrum of such thin layers. This is apparently due to selective resonance enhancement of Raman scattering at the A_1^{LO}(InGaN) polar phonons. Such resonance occurs since the excitation photon energy is close to the energies of real electronic transitions. The electron states involved in the transitions result from nanometer-scaled compositional and strain-induced irregularities in the InGaN QWs, as discussed above.

The experimentally observed gradual decrease (increase) in the frequency of the A_1^{LO}(InGaN) band upon scanning along the direction of growth of the InGaN/GaN SLs unambiguously shows the gradient character of relaxation of elastic compressive strains in the InGaN layers. In this case, the most efficient relaxation of compressive strains occurs in the middle InGaN layers of the SL. The strains in the InGaN layers vary in the range $-(0.9–1.04) \times 10^{-2}$. The effect of relaxation of strains completely correlates with the decrease in the FWHM of the $A_1^{LO}(In_xGa_{1-x}N)$ band. A similar effect of gradient relaxation of compressive strains along the direction of growth was observed recently in the GaN QDs of the 200-period GaN/AlN SL with the GaN QWs by confocal micro-Raman spectroscopy [50].

4. CONCLUSIONS

By high-resolution XRD analysis, the strained state of the SL and constituent individual layers and the degree of relaxation of the buffer have been studied; in addition, the SL period, the layer thicknesses, and the composition of the $In_xGa_{1-x}N$ alloy in the active region have been determined. It is established that, for all of the structures studied here, the GaN layers of the SL are in the stretched state ($\varepsilon_{xx} > 0$) and the alloy layers are in the compressive state ($\varepsilon_{xx} < 0$). In magnitude, the stretching strains of the GaN layers are smaller than the compressive strains of the InGaN layers. For all of the SLs, the relaxation of strains occurs at the lower heterointerface; i.e., the strains produced between the SL as a whole and the buffer layer are removed. It is shown that the layers involved in the SL contain a smaller number of dislocations in comparison to the buffer layers with a more random distribution of dislocations. The insignificant effect of dislocations in the SL is supported also by its state strained relative to the buffer layer.

Confocal micro-Raman spectroscopy of III–N nanostructures makes it possible to obtain unique data on the spatial structural irregularities of the crystal and on the distribution of strains with a submicrometer resolution. Such data are sometimes unobtainable with other experimental techniques. The experimental Raman spectra are indicative of the relatively high quality of the multilayered InGaN/GaN structures.

From the PL and XRD data on the In content x and the strain $\varepsilon_{xx}(x)$ in the plane of the $In_xGa_{1-x}N$ layers of the active region, the frequency shift $\Delta\omega$ of the $A_1^{LO}(In_{0.18}Ga_{0.72}N)$ mode due to elastic strains in the layers is determined: $\Delta\omega = 16.06 \pm 2$ cm^{-1}. This value is in good agreement with the experimental frequency.

Direct evidence for the gradient distribution of strains in depth in the epitaxial layers of the multilayered InGaN/GaN structure is obtained. The broadening of the emission bands due to the nonuniform spatial distribution of indium and strains, as well as due to fluctuations of the QW and barrier thicknesses, is established.

It is shown that a different orientation of crystallites in polycrystalline nitride layers can be responsible for the extra broadening of phonon bands, whereas the strain fields and their nonuniformity influence the width and the frequency position of the bands.

ACKNOWLEDGMENTS

This study was supported in part by the State Foundation for Basic Research of Ukraine, project no. F29.01/015-2009.

REFERENCES

1. S. Nakamura and G. Fasol, *The Blue Laser Diode* (Springer, Berlin, 1997).
2. F. A. Ponce and D. P. Bour, Nature **386**, 351 (1997).
3. G. Popovici, H. Morkoç, and S. N. Mohammad, in *Group III Nitride Semiconductor Compounds: Physics and Applications Ser. on Semiconductor Sci. and Technol.*, v. 6, Ed. by B. Gil (Clarendon, Oxford, 1998), p. 16.
4. C. R. Abernathy, in *GaN and Related Materials*, Ed. by S. J. Pearton (Gordon Breach, New York, 1997), p. 11.

5. M. Asif Khan, Q. Chen, J. Yang, M. Z. Anwar, M. Blasingame, and M. S. Shur, Tech. Dig. Int. Electron Devices Meet. **96**, 27 (1996).
6. Zhenyang Zhong, O. Ambacher, A. Link, V. Holy, J. Stangl, R. T. Lechner, T. Roch, and G. Bauer, Appl. Phys. Lett. **80**, 3521 (2002).
7. L. Kirste, K. M. Pavlov, S. T. Mudie, V. I. Punegov, and N. Herres, J. Appl. Cryst. **38**, 183 (2005).
8. S. Pereira, M. R. Correia, E. Pereira, K. P. O'Donnell, C. Trager-Cowan, F. Sweeney, and E. Alves, Phys. Rev. B **64**, 205311 (2001).
9. S. Pereira, E. Pereira, E. Alves, N. P. Barradas, K. P. O'Donnell, C. Liu, C. Deatcher, and I. M. Watson, Appl. Phys. Lett. **81**, 2950 (2002).
10. J. Frandon, I. M. Watson, C. Liu, E. Alves, A. D. Sequeira, and N. Franco, Appl. Phys. Lett. **85**, 2235 (2004).
11. Y. Narukawa, S. Saijou, Y. Kawakami, S. Fujita, T. Mukai, and S. Nakamura, Appl. Phys. Lett. **74**, 558 (1999).
12. Chih-Feng Lu, Chi-Feng Huang, Yung-Sheng Chen, and C. C. Yang, J. Appl. Phys. **104**, 043108 (2008).
13. I. P. Soshnikov, V. V. Lundin, A. S. Usikov, I. P. Kalmykova, N. N. Ledentsov, A. Rosenauer, B. Neubauer, and D. Gerthsen, Fiz. Tekh. Poluprovodn. **34**, 647 (2000) [Semiconductors **34**, 621 (2000)].
14. M. R. Correia, S. Pereira, E. Pereira, J. Frandon, and E. Alves, Appl. Phys. Lett. **83**, 4761 (2003).
15. V. P. Kladko, A. F. Kolomys, M. V. Slobodian, V. V. Strelchuk, V. G. Raycheva, A. E. Belyaev, S. S. Bukalov, H. Hardtdegen, V. A. Sydoruk, N. Klein, and S. A. Vitusevich, J. Appl. Phys. **105**, 063515 (2009).
16. W. Qian, M. Skowronski, M. De Graef, K. Doverspike, L. B. Rowland, and D. K. Gaskil, Appl. Phys. Lett. **66**, 1252 (1995).
17. D. Behr, J. Wagner, A. Ramakrishnan, H. Obloh, and K.-H. Bachem, Appl. Phys. Lett. **73**, 241 (1998).
18. M. Yamaguchi, T. Yagi, T. Sota, T. Deguchi, K. Shimada, and S. Nakamura, J. Appl. Phys. **85**, 8502 (1999).
19. W. Paszkowicz, Powder Diffract. **14**, 258 (1999).
20. V. S. Speriosu and T. Vreeland, Jr., J. Appl. Phys. **56**, 1591 (1984).
21. V. P. Kladko, A. V. Kuchuk, N. V. Safryuk, V. F. Machulin, A. E. Belyaev, R. V. Konakova, and B. S. Yavich, Semicond. Phys. Quant. Electron. Optoelectron. **13**, 1 (2010).
22. R. N. Kyutt, M. L. Shcheglov, V. Yu. Davydov, and A. S. Usikov, Fiz. Tverd. Tela **46**, 353 (2004) [Phys. Solid State **46**, 364 (2004)].
23. V. P. Kladko, A. V. Kuchuk, N. V. Safryuk, V. F. Machulin, A. E. Belyaev, H. Hardtdegen, and S. A. Vitusevich, Appl. Phys. Lett. **95**, 031907 (2009).
24. V. P. Klad'ko, S. V. Chornen'kiĭ, A. V. Naumov, A. V. Komarov, M. Takano, Yu. N. Sveshnikov, S. A. Vitusevich, and A. E. Belyaev, Fiz. Tekh. Poluprovodn. **40**, 1087 (2006) [Semiconductors **40**, 1060 (2006)].
25. C. C. Chuo, C. M. Lee, T. E. Nee, and J. I. Chyi, Appl. Phys. Lett. **76**, 3902 (2000).
26. J. P. Donnelly and A. G. Milnes, IEEE Trans. Electron. Dev. ED **14**, 63 (1967).
27. J. Christen and D. Bimberg, Phys. Rev. B **42**, 7213 (1990).
28. W. Hayers and R. Laudon, *Scattering of Light by Crystals* (Wiley, New York, 1978).
29. T. Azuhata, T. Sota, K. Suzuki, and S. Nakamura, J. Phys.: Condens. Matter **7**, L129 (1995).
30. Y. T. Songa, X. L. Chen, W. J. Wang, W. X. Yuan, Y. G. Cao, and X. Wu, J. Cryst. Growth **260**, 327 (2004).
31. H. Grille, C. Schnittler, and F. Bechstedt, Phys. Rev. B **61**, 6091 (2000).
32. A. G. Kontos, Y. S. Raptis, N. T. Pelekanos, A. Georgakilas, E. Bellet-Amalric, and D. Jalabert, Phys. Rev. B **72**, 155336 (2005).
33. Keunjoo Kim, Appl. Phys. Lett. **90**, 012116 (2007).
34. M. Ya. Valakh, N. O. Korsunska, Yu. G. Sadofyev, V. V. Strelchuk, G. N. Semenova, L. V. Borkovska, V. V. Artamonov, and M. V. Vuychik, Mater. Sci. Eng. B **101**, 255 (2003).
35. V. Yu. Davydov and A. A. Klochikhin, Fiz. Tekh. Poluprovodn. **38**, 897 (2004) [Semiconductors **38**, 861 (2004)].
36. L. Bergman, D. Alexson, P. L. Murphy, R. J. Nemanich, M. Dutta, M. A. Stroscio, C. Balkas, H. Shin, and R. F. Davis, Phys. Rev. B **59**, 12977 (1999).
37. J. Ibanez, R. Cusco, L. Artus, M. Henini, and A. Patane, L. Eaves. Appl. Phys. Lett. **88**, 141905 (2006).
38. R. Loudon, Adv. Phys. **13**, 423 (1964).
39. L. Shi, F. A. Ponce, and J. Menendez, Appl. Phys. Lett. **84**, 3471 (2004).
40. J. H. Campbell and P. M. Fauchet, Solid State Commun. **58**, 10739 (1986).
41. A. Cros, N. Garro, J. M. Llorens, A. Garsia-Cristobal, A. Cantarero, N. Gogneau, E. Monroy, and B. Daudin, Phys. Rev. B **73**, 115313 (2006).
42. T. Ruf, J. Serrano, M. Cardona, P. Pavone, M. Pabst, M. Krisch, M. D'Astuto, T. Suski, I. Grzegory, and M. Leszczynski, Phys. Rev. Lett. **86**, 906 (2001).
43. V. A. Fonoberov and A. A. Balandin, J. Phys.: Condens. Matter **17**, 1085 (2005).
44. A. Cros, N. Garro, A. Cantarero, J. Coraux, H. Renevier, and B. Daudin, Phys. Rev. B **76**, 165403 (2007).
45. T. Yamanaka, D. Alexson, M. A. Stroscio, M. Dutta, P. Petroff, J. Brown, and J. Speck, J. Appl. Phys. **104**, 093512 (2008).
46. F. Demangeot, J. Frandon, P. Baules, F. Natali, F. Semond, and J. Massies, Phys. Rev. B **69**, 155215 (2004).
47. N. Wieser, O. Ambacher, H.-P. Felsl, L. Görgens, and M. Stutzmann, Appl. Phys. Lett. **74**, 3981 (1999).
48. V. Yu. Davydov, A. A. Klochikhin, I. N. Goncharuk, A. N. Smirnov, A. V. Sakharov, A. P. Skvortsov, M. A. Yagovkina, V. M. Lebedev, H. Lu, and W. J. Schaff, Phys. Stat. Solidi B **243**, 1494 (2006).
49. K. Kisoda, K. Hirakura, and H. Harima, Phys. Stat. Solidi C **3**, 1997 (2006).
50. A. Cros, J. Fresneda, J. A. Budagovsky, B. Amstatt, and B. Daudin, Phys. Stat. Solidi B **246**, 1191 (2009).

Translated by É. Smorgonskaya